Element stiffness matrix integration in *image-based* Cartesian Grid Finite Element Method

Luca Giovannelli, Juan J. Ródenas, José M. Navarro-Jimenez and Manuel Tur

Centro de Investigación en Tecnología de Vehículos,
Universitat Politècnica de València, Spain
jjrodena@mcm.upv.es

Abstract. Following traditional methods, before a FE model can be obtained, patient specific FE simulations usually require a time consuming, often manual, preliminary stage of segmentation and geometry creation in order to obtain a CAD model from the medical image, suitable to be meshed. The most common alternative is the direct creation of a uniform hexahedral mesh in which each pixel/voxel perfectly fits one element. The main drawback of this method is the great number of degrees of freedom in the FE mesh, which makes it challenging to solve the numerical problem due to the high computational cost. *Image-based* Cartesian grid Finite Element Method (*image-based* cgFEM) is a technique which allows to obtain h-adaptive Finite Element (FE) models with a reasonable number of degrees of freedom from images in an automatic way without the necessity of creating an intermediate geometrical model. Thus cgFEM represents an alternative to maintain accuracy with a low computational cost. In cgFEM the image is directly immersed into an initial uniform Cartesian mesh. The hierarchical structure of nested Cartesian grids on which cgFEM is based allows a fast and efficient h-adaptive process to be carried out in order to adapt the mesh to the bitmap representation of the body to simulate. The h-refinement process is performed by element splitting and guided by the evaluation of the pixel value distribution. In this paper a comparison between different integration strategies are presented for the calculation of the element stiffness matrices in *image-based* cgFEM. These are a special integration technique based on the Riemann sum, one based on the standard Gauss quadrature applied on subdomains coinciding with the pixels, a Gauss quadrature of the whole element domain in which the material property field is interpolated using Least Squares (LS) fitting or by Superconvergent Patch Recovery (SPR).

1 Introduction

Medical imaging has a key role in patient-specific treatment, [1], as shown by the great amount of publications on this topic. Intense research has been devoted to find new ways of taking advantage of the information provided by medical images. As a consequence, a large number of new applications based on the use

of computational tools have been proposed in many different fields such as the prediction of bone fracture risk, [2], the reduction of surgery invasiveness, [3], prosthesis selection, [4], and the evaluation of bone quality parameters for the detection of osteoporosis, [5]. Many applications in which it is necessary to compute mechanical quantities of biological structures in a patient specific framework are at the crossroads between these image based applications and the area of computational mechanics, traditionally linked to industrial production. This is the case of bone mechanics for instance. A rich literature exists about creation of numerical models derived from computational mechanics from medical images for specific applications, such as, for instance, [6]. Most of these techniques use the Finite Element Method (FEM), as this is the most spread numerical tool for structural simulation. Traditional patient specific medical FEM applications can be classified into two main categories [7]. We call the methods belonging to the first one *image-based*, since they take advantage of the regular spatial distribution of the pixels/voxels to directly assign a Finite Element (FE), usually hexahedral, to each of them. The first step is usually a segmentation procedure to select the pixels of interest, afterwords the mesh creation is straightforward. This technique automatically provides uniform structured meshes which present some advantages from the point of view of information treatment due to the similarities between all the elements. In addition, if local material properties have to be taken into account, information transfer between image and mesh is very easy due to the biunivocal correspondence between elements and pixels. The main price to pay for using this method is the great amount of degrees freedom of the final problem, which can be computationally very expensive.

The second family, which we call *geometry-based*, use procedures to create CAD models from image data. Afterwords, the modeling and simulating processes used are exactly the same as in standard FEM problems. On one hand this means that the tools and techniques used for FE modeling in structural analysis can be easily extended to the patient specific problem. Doing so, problems with a reasonable number of degrees of freedom can usually be obtained. On the other hand, some typical modeling problems related to complex geometries may appear. On this point note that in usual structural simulations, the phases of adapting CAD models to FE domain discretization and meshing are responsible on average for about 80% of all the time cost, [8].

The main drawback of the *geometry-based* methods is not in modeling and simulation, yet in the creation of the CAD model from the original image. This process requires cumbersome and time consuming techniques of segmentation and geometry creation which can be seldom completely automatic, hence resulting in high costs in terms of highly specialized man-hours. In addition, including local information into the simulation is difficult in the general case for FE models thus obtained, as the mesh and bitmap topologies are totally independent.

Recently, in order to overcome the limits of both *image-* and *geometry-based* procedures, advanced FE methods, formerly developed for lightening the meshing and remeshing burden in standard geometrical problems, have been extended

to this area, such as the Extended Finite Element Method (XFEM) [9] or the Finite Cell Method (FCM) [10].

Our proposal is an advanced FE method for performing linear elasticity analyses in the case the problem data are available in the form of bitmaps. We call this method *image-based* Cartesian grid Finite Element Method (*image-based* cgFEM). cgFEM provides meshes characterized by a reasonable number of degrees of freedom, as in the *geometry-based* procedures, but, at the same time, no CAD model to mesh has to be created and all the local pixel information can be used, as in *image-based* procedures, [11]. It has points in common especially with FCM, since both methods create regular square/hexahedral meshes directly inside the bitmap and, as a consequence, have to use special techniques for enforcing Dirichlet boundary condition on surfaces which cut the elements. The main difference is in the mesh refinement procedures. FCM enhances the FE solution by performing p-refinement, that is by increasing the polynomial order of the shape functions used for interpolating the displacement field and has to deal with their proper integration, while, in contrast, in cgFEM the model is refined via local local h-adaptivity, hence reducing the element size on the basis of the evaluation of the variability of the pixel value field.

As in usual FEM, in *image-based* cgFEM it is necessary to compute the integral (1) for each element of the mesh in order to be able to assemble the element stiffness matrices $\mathbf{k}^e$ into the problem global stiffness matrix $\mathbf{K}$.

$$\mathbf{k}^e = \int_{\Omega} \mathbf{B}^T \mathbf{D} \mathbf{B} \mathrm{d}\Omega \tag{1}$$

In (1), whose evaluation is performed by numerical integration , $\mathbf{B}$ is the matrix relating strains and nodal displacements, $\mathbf{D}$ the Hook's law matrix which relates strains and stresses in linear elasticity. As opposed to usual FEM, in which only $\mathbf{B}$ depends on the position, in *image-based* cgFEM the $\mathbf{D}$ matrix also does. This is due to the fact that, in general, the material inside each element is not homogeneous. This heterogeneity is only sampled at the centers of the pixels, therefore, in order not to lose information, it is necessary to take into account all the pixels during the simulation. In cgFEM this information is included by considering all the pixels for homogenizing the elastic properties at the element level. As a consequence each element contains a number of pixels, hence significantly reducing the number of degrees of freedom because in the final model there are significantly less elements than pixels, in contrast to the classical *image-based* methods. The aim of the previous adaptivity process is avoiding excessive homogenization of the material properties inside each element. Due to the specific features of the procedure, the numerical integration is not standard. In this paper, we propose and compare different strategies for carrying out the integral (1) in the context of image-based cgFEM. They can be divided in two classes:

- Strategies based on the direct use of the whole image information
  - Riemann Sum based technique
  - Gauss quadrature in subdomains of integration

– Strategies based on the reconstruction of a continuous elastic property distribution inside each element
  • Least Square fitting (LS) to pixel field
  • Superconvergent Patch Recovery (SPR) fitting to pixel field

After this introduction, in Section 2 the *image-based* cgFEM technique, the different integration techniques and the test problem are presented followed by the numerical results in Section 3. Finally, Section 4 is devoted to the discussion of the results and the formulation of the conclusions.

2 Method

2.1 *Image-based* cgFEM

FE modeling in linear elasticity consists mainly of three steps: domain discretization, stiffness matrix calculation and imposition of the boundary conditions. In cgFEM, a hierarchical structure of nested Cartesian grids is used for making meshing and h-refinement efficient, [12]. This consists of a series of Cartesian grids in which the first one, so called 0 *level*, only consists of one single element coinciding with the bounding box which contains the domain of interest, see Figure 1. The i-level grid is then obtained by splitting each element of the

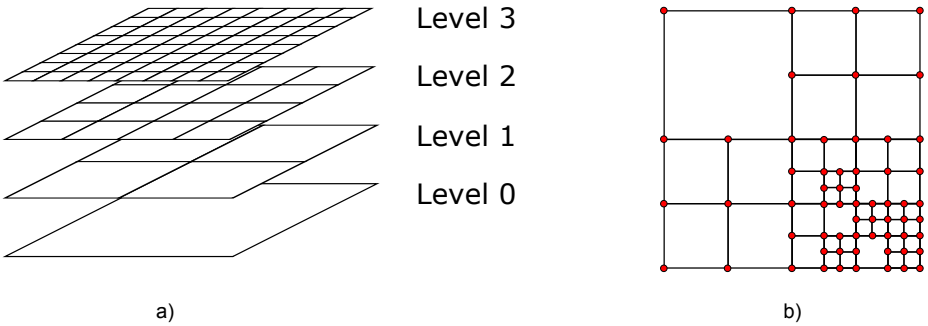

Fig. 1. a) First levels of the hierarchical structure of nested Cartesian grids; b) Example of non-conforming Finite Element mesh with cgFEM

$i-1$-level in two in each direction, therefore it contains $2^{d\times i}$ elements, in which d represent the problem dimensionality. The final mesh is created by assembling

elements from different levels. This is computationally efficient because the elements are related by parenthood and neighborhood relations known in advance, therefore the amount of data to store decreases. The FE mesh, thus obtained, has hanging nodes at which the displacement field continuity has to be enforced by using Multi Point Constraints (MPC). The level difference between two adjacent elements is enforced not to be more of one level.

At the beginning of the simulation, the image is reshaped, usually adding *dummy* pixels, so that its dimensions, measured in pixels, are powers of two along each direction. This guarantees that, in the hierarchical structure of Cartesian grids, a number of levels exist in which all the elements contain an integer number of pixels. This makes the process of structuring the image into the mesh straightforward. The second step is to h-refine the mesh by evaluating the pixel value distribution in each element. For this purpose the ratio between the element and the whole image value range or the coefficient of variation, the ratio between the image value standard deviation and its mean value have been considered. Once the problem has been discretized, the element stiffness matrix (1) is numerically calculated by using (2).

$$\mathbf{k}^e = \sum_{i=1}^{IP} \mathbf{B}^T(\boldsymbol{\xi}_i)\mathbf{D}(\boldsymbol{\xi}_i)\mathbf{B}(\boldsymbol{\xi}_i) \mid \mathbf{J}(\boldsymbol{\xi}_i) \mid w_i \tag{2}$$

In which the number of the integration points IP, their positions $\boldsymbol{\xi}_i$ (corresponding in 2D with the vector (ξ_i, η_i), in 3D with(ξ_i, η_i, τ_i)), the Jacobian $\mid \mathbf{J}(\boldsymbol{\xi}_i) \mid$, the weights and the material property values $\mathbf{D}(\boldsymbol{\xi}_i)$ depend on the quadrature rule chosen.

2.2 Pixel based integration methods

In this group of integration strategies, no treatment of the image is performed and the values of $\mathbf{D}$ introduced in (2) are directly the ones of the pixels.

Pixels as subdomains of integration. A first approach consists of considering the pixels as element integration subdomains in which the values of $\mathbf{D}$ are constant over the subdomain, therefore a proper Gauss integration has to be performed in each pixel. As a result the number of integration points IP required in each element is $NP \times GIP$, where NP is the number of pixels contained in the element and GIP the number of integration points required by the Gauss quadrature for an homogeneous domain.

$$\mathbf{k}^e = \sum_{j=1}^{Pixels} \sum_{i=1}^{IP} \mathbf{B}^T(\boldsymbol{\xi}_i)\mathbf{D}_j\mathbf{B}(\boldsymbol{\xi}_i) \mid \mathbf{J}_{ij}(\boldsymbol{\xi}_i) \mid w_i \tag{3}$$

Riemann sum based integration. The second approach consists of implementing Riemann sum hence locating one constant weight integration point at the center of each pixel.

$$\mathbf{k}^e = \sum_{i=1}^{IP} \mathbf{B}^T(\boldsymbol{\xi}_i)\mathbf{D}_i\mathbf{B}(\boldsymbol{\xi}_i)PA_i \tag{4}$$

in which PA_i is the measure of the pixel area in global coordinates.

2.3 Recovered image integration methods

In this second group, a continuous material property field is used to interpolate the values of the pixels, therefore the proper Gauss quadrature 5 is used.

$$\mathbf{k}^e = \sum_{i=1}^{GP} \mathbf{B}^T(\boldsymbol{\xi}_i)\mathbf{D}(\boldsymbol{\xi}_i)\mathbf{B}(\boldsymbol{\xi}_i) \mid \mathbf{J}_{ij}(\boldsymbol{\xi}_i) \mid w_i \tag{5}$$

Least Square recovery. Least Square techniques provides a polynomial interpolation $f(\boldsymbol{\xi}_i) = \mathbf{p}(\boldsymbol{\xi}_i)\mathbf{a}$ of the material property field in each element. This is, in general, discontinuous at the interface between two adjacent elements and is obtained by minimizing the function Π (6) with respect to each one of the polynomial coefficients a_i (7), which leads to a linear system of equations that is used to evaluate $\mathbf{a}$.

$$\Pi = \sum_{i}^{Pixels} (PV_i - f(\boldsymbol{\xi}_i))^2 = \sum_{i}^{Pixels} (PV_i - \mathbf{p}(\boldsymbol{\xi}_i)\mathbf{a})^2 \tag{6}$$

$$\frac{\partial \Pi}{\partial a_i} = 0 \tag{7}$$

In the following, for simplicity, we only consider that p represents a bilinear polynomial basis.

SPR recovery. The SPR recovery [13] uses a Least Square polynomial fitting to the values of the pixels contained in a patch. A patch is the set of the elements which share the same node. The fitted polynomial is then used to evaluate the material property value at the common node of the patch $\mathbf{D}_i$. These nodal values are then used for calculating the values at the Gauss points by FE interpolation, see (8)

$$\mathbf{D}(\boldsymbol{\xi}_i) = \sum_{j}^{Nodes} N_j(\boldsymbol{\xi}_i)\mathbf{D}_j \tag{8}$$

The resulting field is continuous over the whole mesh.

2.4 Reference Problem

The different integration techniques have been compared on a reference problem. For the sake of simplicity we use the 2D image of a phalanx, Figure 2 b), from the x-ray image of a finger expressed grey scale (with values from 0 to 255), see Figure 2 a).

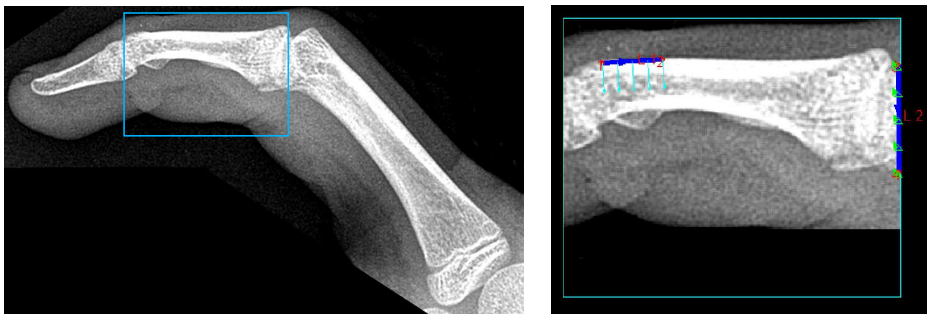

Fig. 2. a) X-ray image of a finger; b) Reference problem: phalanx from the hand X-ray in Figure 2

Material	**E [MPa]**	ν	**Gray level**
Material 1	0	0.0	0
Material 2	645	0.43	150
Material 3	14000	0.3	190
Material 4	14200	0.3	255

Table 1. Material Properties used for the convergence study.

The relation between the pixel values and the material elastic properties were assigned by associating data from the literature, [14] and [15], to certain values of the gray scale, see Table 1. For the rest of the gray scale, linear interpolation was used.

3 Numerical Results

Our reference solution corresponds to the energy norm evaluated considering one element per pixel in the image, considering also 4 integration points per element (pixel) to ensure that the numerical integration (1) is exact. Our goal is to check which of the integration methods provides the energy norm values closest to the reference solution at the minimum computational cost. To do so, we will first check the evolution of the solution obtained with each one of the different techniques, considering uniform mesh refinement with meshes with 8×8, 4×4, 2×2 and 1×1 pixels per element. Then we will select the most accurate technique to evaluate further improvements in computational cost associated to h-adaptive mesh refinement. Figure 3 shows the FE energy norm, $\sqrt{\int_\Omega \boldsymbol{\sigma} \mathbf{D}^{-1} \boldsymbol{\sigma} dV}$, of the reference problem for increasingly refined homogeneous meshes. Figures 3 a) and b) represent the energy norm versus the total number of degrees of freedom and integration points respectively. Note that both parameters are relevant for the computational efficiency because, on one hand, the computational cost required for solving the system of equations associated to the FE problem depends on the number of degrees of freedom and, on the other hand, the effort associated to the creation of the system of equations increases with the number of integration points. In Figure 3 c) the difference with the energy norm of the reference solution is used as a measure of the error. The blue line in Figures 3 a), b) and c) represent the integration by decomposition of the elements into subdomains of integration treated with the proper Gauss quadrature of four integration points. It converges smoothly to the reference solution since its finest mesh corresponds with the reference solution. The number of integration points involved is high and independent from the mesh. The results obtained by using the Riemann sum integration is shown in red in Figure 3. Its behavior is very close to the previous one descending from the decomposition in subdomains as far as at least 4 integration points are contained in each element. In the most refined mesh the Riemann sum based technique coincides with a reduced integration of one Gauss point and, as a consequence, the error suddenly increases. Note that for coarser meshes, the method provides almost the same accuracy as the the integration subdomain decomposition with 1/4 of the integration points. The SPR technique, the green line, shows very low values of the error in the coarser mesh, but an unstable behavior along the mesh refinement with the highest value of error for its finest mesh. This unstable behavior has also been observed in other numerical tests. SPR is not a reliable method for this application because it provides continuous fields along adjacent elements. This characteristic smooths the material property too much between different tissues in the X-ray image. Finally, the integration of the LS interpolation, violet curve, shows the best behavior: it

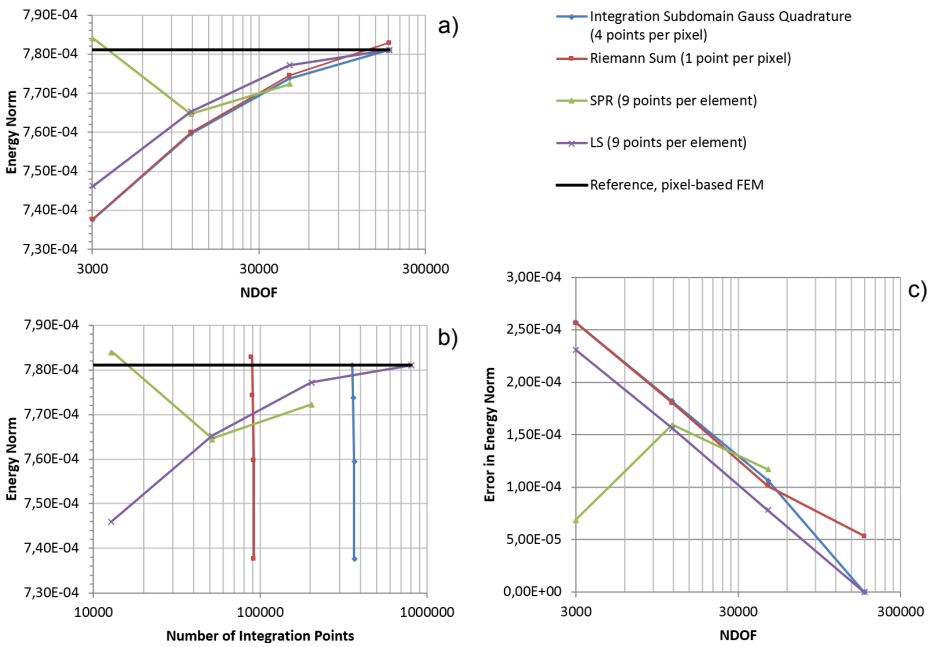

Fig. 3. a) Reference Problem Energy Norm vs Degrees of freedom; b) Reference Problem Energy Norm vs Integration points; c) Reference Problem Error vs Degrees of Freedom

is not only characterized by higher accuracy than all the other methods, converging correctly to the reference solution, but over a certain element size it is also cheaper from the point of view of the number of integration points. This good behavior is probably due to the fact that the bilinear LS interpolation of the material properties is consistent with the linear shape functions used for the FE interpolation of the displacement field. In addition the method filters the image high frequency noise taking into account only the low frequencies, in the process only most important information is taken into account with a reduced number of degrees of freedom. Since the LS based integration technique proved to be the best one in the reference problem, it was used for comparing the behaviors of cgFEM h-adaptive approach and uniform refinement for the previous problem. In the results shown in Figure 4 the h-adaptivity is guided by the evaluation of the pixel value variability. This is limited by element splitting.

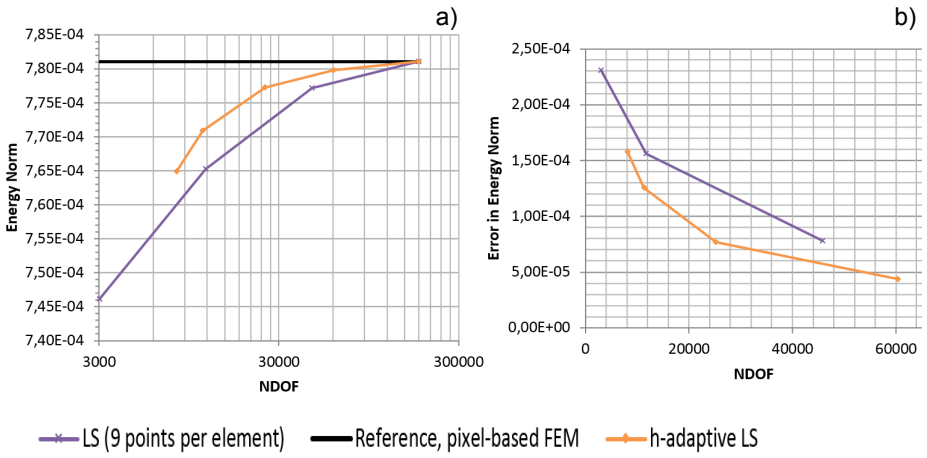

Fig. 4. a) H-adaptive refinement vs uniform refinement. Energy Norm vs Degrees of freedom; b) Error in energy norm

Doing so the number of degrees of freedom is only increased where the material heterogeneity requires so. The difference between an adapted mesh with a certain number of degrees of freedom and the next one with a higher number of degrees of freedom is in the variability threshold which guides the refinement. The h-adapted meshes corresponding to the points on the yellow curve in the Figure 4 are shown in the Figure 5. Figure 4 shows a relevant difference in the number of degrees of freedom, and hence in the computational cost, between the two methods for similar accuracies. This results suggest that, if used together with the proper integration method, h-refined *image-based*cgFEM models can be used for increasing patient specific simulation efficiency.

4 Conclusions

The *image-based* cgFEM technique has been presented and different techniques for the integration of element stiffness matrices evaluated from medical images have been compared. There are negligible differences between the technique based on the Riemann sum and the one based on integration subdomain decomposition, computationally more expensive. The former only provides less accurate results for elements containing one single pixel. Both methods have

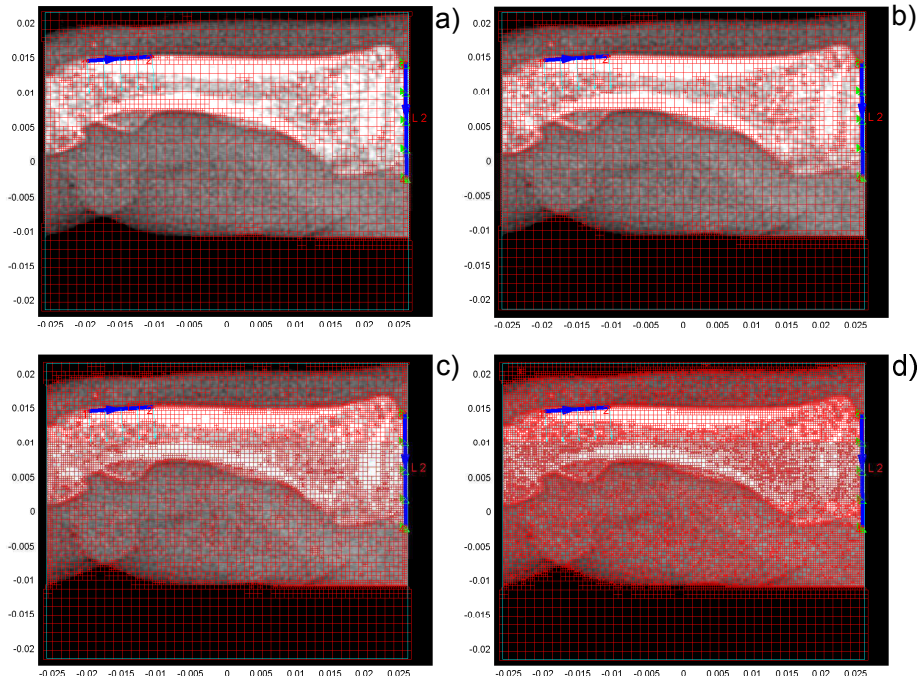

Fig. 5. Meshes created during the h-adaptive strategy corresponding to the yellow curves in Figure 4

a constant number of integration points independent from the mesh. The use of SPR provides unstable convergence curves and showed not to be a reliable method for this application. The best and computationally cheapest results, were obtained by LS. This was also used together with an heterogeneity based h-adaptive technique to show the higher accuracy and computational efficiency with respect to the uniform refinement.

Acknowledgements

With the support of the European Union Framework Program (FP7) under grant agreement No. 289361 'Integrating Numerical Simulation and Geometric Design Technology (INSIST)'and Generalitat Valenciana (PROMETEO/2012/023).

References

1. Neal, M.L., Kerckhoffs, R.: Current progress in patient-specific modeling. Briefings in Bioinformatics **11**(1) (January 2010) 111–126
2. Grassi, L., Schileo, E., Taddei, F., Zani, L., Juszczyk, M., Cristofolini, L.: Accuracy of finite element predictions in sideways load configurations for the proximal human femur. Journal of biomechanics **45**(2) (2012) 394–399
3. Viceconti, M., Lattanzi, R., Antonietti, B., Paderni, S., Olmi, R., Sudanese, A., Toni, A.: CT-based surgical planning software improves the accuracy of total hip replacement preoperative planning. Medical Engineering & Physics **25**(5) (June 2003) 371–377
4. Bongini, D., Carfagni, M., Governi, L.: Hippin: a semiautomatic computer program for selecting hip prosthesis femoral components. Computer methods and programs in biomedicine **63**(2) (October 2000) 105–15
5. Alberich-Bayarri, A., Marti-Bonmati, L., Sanz-Requena, R., Belloch, E., Moratal, D.: In vivo trabecular bone morphologic and mechanical relationship using high-resolution 3-T MRI. AJR. American journal of roentgenology **191**(3) (September 2008) 721–6
6. García-Aznar, J.M., Bayod, J., Rosas, A., Larrainzar, R., García-Bógalo, R., Doblaré, M., Llanos, L.F.: Load transfer mechanism for different metatarsal geometries: A finite element study. Journal of Biomechanical Engineering **131**(2) (2009)
7. Viceconti, M.: A comparative study on different methods of automatic mesh generation of human femurs: Medical Engineering and Physics 20 (1998):1-10 [1]. Medical Engineering and Physics **22**(5) (2000) 379–380
8. Cottrell, J.A., Hughes, T.J.R., Bazilevs, Y.: Isogeometric Analysis: Toward Integration of CAD and FEA. 1st edn. Wiley (2009)
9. Lian, W.D., Legrain, G., Cartraud, P.: Image-based computational homogenization and localization: Comparison between X-FEM/levelset and voxel-based approaches. Computational Mechanics **51**(3) (May 2013) 279–293
10. Ruess, M., Tal, D., Trabelsi, N., Yosibash, Z., Rank, E.: The finite cell method for bone simulations: verification and validation. Biomechanics and modeling in mechanobiology **11**(3-4) (March 2012) 425–37
11. Giovannelli, L., Marco, O., Navarro, J.M., Giner, E., Ródenas, J.J.: Direct Creation of Finite Element Models from Medical Images using Cartesian Grids. In: Computational Vision and Medical Image Processing, IV ECCOMAS thematic conference on computational vision and medical image processing, VipIMAGE. (2013)
12. Nadal, E.: On the use of Cartesian Grid Finite Element codes in structural optimization. (October) (2012)
13. Zienkiewicz, O.C., Zhu, J.Z.: The superconvergent patch recovery and a posteriori error estimates. part 1: The recovery technique. International Journal for Numerical Methods in Engineering **33**(7) (1992) 1331–1364
14. Viceconti, M., Bellingeri, L., Cristofolini, L., Toni, A.: A comparative study on different methods of automatic mesh generation of human femurs. Medical engineering & physics **20**(1) (January 1998) 1–10
15. Kim, H., Jürgens, P., Weber, S., Nolte, L.P., Reyes, M.: A new soft-tissue simulation strategy for cranio-maxillofacial surgery using facial muscle template model. Progress in biophysics and molecular biology **103**(2-3) (December 2010) 284–91